Original Article

Isoprenyl phenolic ethers from the termite nest-derived medicinal fungus *Xylaria fimbriata*

Mei-Chuan Chen [a,b], Guei-Jane Wang [c,d,e], Yueh-Hsiung Kuo [f,g],
Yin-Ru Chiang [h], Ting-Yu Cho [a], Yu-Ming Ju [i], Tzong-Huei Lee [j,*]

[a] Graduate Institute of Pharmacognosy, Taipei, Taiwan
[b] The Ph.D. Program for the Clinical Drug Discovery from Botanical Herbs, Taipei Medical University, Taipei, Taiwan
[c] School of Medicine, Graduate Institute of Clinical Medical Science and Biomedical Sciences, China Medical University, Taichung, Taiwan
[d] Department of Medical Research, China Medical University Hospital, Taichung, Taiwan
[e] Department of Health and Nutrition Biotechnology, Asia University, Taichung, Taiwan
[f] Department of Chinese Pharmaceutical Sciences and Chinese Medicine Resources, China Medical University, Taichung, Taiwan
[g] Department of Biotechnology, Asia University, Taichung, Taiwan
[h] Biodiversity Research Center, Academia Sinica, Taipei, Taiwan
[i] Institute of Plant and Microbial Biology, Academia Sinica, Taipei, Taiwan
[j] Institute of Fisheries Science, National Taiwan University, Taipei, Taiwan

ARTICLE INFO

ABSTRACT

Seven new isoprenyl phenolic ethers, namely fimbriethers A–G (**1–7**), were isolated from the fermented broth of the termite nest-derived medicinal fungus *Xylaria fimbriata* YMJ491. Their structures were determined by spectroscopic data analysis and compared with those reported. The effects of all the isolates at a concentration of 100 μM on the inhibition of nitric oxide (NO) production in lipopolysaccharide (LPS)-induced murine macrophage RAW 264.7 cells were evaluated, and all of them exhibited NO production inhibitory activity with E_{max} values ranging from 4.6 ± 2.0% to 49.7 ± 0.5% without significant cytotoxicity. In addition, these seven compounds did not alter phenylephrine-induced vasocontraction in isolated intact thoracic aortic rings from C57BL/6J mouse, indicating **1–7** were not involved in the regulation of endothelial NOS-mediated NO production.

* Corresponding author. Institute of Fisheries Science, National Taiwan University, No.1, Sec. 4, Roosevelt Rd., Taipei, 10617, Taiwan.
  E-mail address: thlee1@ntu.edu.tw (T.-H. Lee).

1. Introduction

There are around 330 species of fungus-growing termites classified in the family of Microtermitinae in the world [1,2]. In Taiwan, the only termite *Odontotermes formmosanus* cultivates an edible basidiomycetous fungus *Termitomyces eurrhizus* and maintains a mutualistically symbiotic relationship between each other [3]. In addition to *Termitomyces*, there are also many other microbes found in the termite nests, e.g. *Xylaria* spp. (Xylariaceae), whose physiological properties were considered to be highly involved with the growth and development of *Termitomyces* [4]. The traditional Chinese Medicine Wu-Ling-Shen refers to the sclerotia of *Xylaria* spp. collected from the abandoned termite nests [5]. However, the field-collected sclerotia are too rare to be industrialized. In an attempt to search for materials which could substitute for sclerotia of *Xylaria* spp., the fermented mycelia or broths of the genus *Xylaria* have been found to display anti-inflammatory [3], cytotoxic [3], antifungal [6], antibacterial [7], antimalarial [8], α-glucosidase inhibitory [8], antinematode [9], and neuro-protective activity [10]. In the recent past, a number of new bioactive principles have been disclosed continuously from *Xylaria* spp. [11–15], which indicated that this fungal genus could be a promising source for developing medicinally useful compounds. In addition, it has been shown that the ethyl acetate extract (100 μg/mL) of the fermented broth of *X. fimbriata* YMJ491 exhibits 100% inhibition of nitric oxide (NO) production in lipopolysaccharide (LPS)-activated murine macrophage RAW264.7 cells in the previous study. Thus, a series of chemical investigation on the extract of the fermented broth of this fungal strain is undertaken, and which has led to the isolation and characterization of seven new isoprenyl phenolic ethers 1–7 (Fig. 1). Herein, we report the structural elucidation of seven new compounds, and their anti-inflammatory effects.

2. Materials and methods

2.1. General experimental procedures

Optical rotations were measured on a JASCO P-2000 polarimeter (Tokyo, Japan). ^1H and ^{13}C NMR were acquired on a Bruker AVIII-500 spectrometer (Ettlingen, Germany). Low and high resolution mass spectra were obtained using an API 4000 triple quadrupole mass spectrometer (Applied Biosystems, Foster City, CA, USA) and Synapt High Definition Mass Spectrometry system with an ESI interface and a TOF analyzer (Waters Corp., Manchester, UK), respectively. IR spectra were recorded on a JASCO FT/IR 4100 spectrometer (Tokyo, Japan). UV spectra were measured on a Thermo UV–Vis Helios α Spectrophotometer (Thermo Scientific, Waltham, MA, USA). Sephadex LH-20 (GE Healthcare Life Sciences, Pittsburgh, PA, USA) was used for open column chromatography. TLC was performed using silica gel 60 F_{254} plates (200 μm, Merck). Reflective index detector (Bischoff, Leonberg, Germany) was used in HPLC purification.

2.2. Fermentation of Xylaria fimbriata YMJ491

X. fimbriata YMJ491 was isolated and identified by one of us (YMJu) [16]. ITS sequences of nuclear ribosomal DNA of this fungal strain were submitted to GenBank, and the accession number was GU324753.1. The mycelium of this strain was inoculated into 5 L serum bottles, each containing 60 g Bacto™ Malt Extract (Becton, Dickinson and Company, Sparks, USA) and 3 L deionized water. The fermentation was conducted with aeration at 25–30 °C for 30 days.

2.3. Extraction and isolation

The filtered fermented broth (15 L) of *X. fimbriata* YMJ491 was partitioned two times with equal volumes of ethyl acetate, then concentrated in vacuum to dryness (4.0 g). The crude extract was re-dissolved in 20 mL MeOH, then applied onto a Sephadex LH-20 column (2.5 cm i.d. × 69.5 cm) and eluted by MeOH with a flow rate of 2.4 mL/min. Each fraction (20 mL) collected was checked for its compositions by TLC using $CHCl_3$–MeOH (10:1, v/v) for development, and dipping in vanillin-sulfuric acid was used to detect compounds with similar chromophores. All the fractions were combined into nine portions I–IX. The portion II (fr. 10–14) was further separated by Diaion HP-20 column (5.0 cm i.d. × 18.0 cm) and eluted by 30% $MeOH_{aq}$, 50% $MeOH_{aq}$, 70% $MeOH_{aq}$, and MeOH in a step-wise gradient mode. Four subportions II-1–II-4 (each 900 mL) collected were checked for their compositions by TLC using $CHCl_3$–MeOH (10:1, v/v) for development. HPLC of
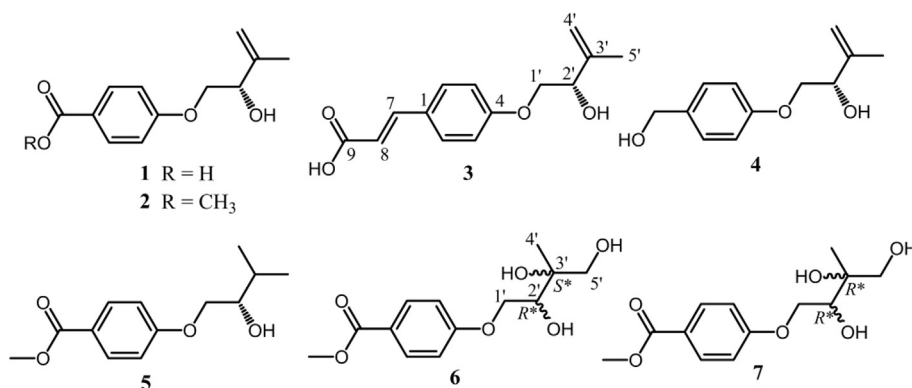

Fig. 1 – Chemical structures of compounds 1–7 identified in this report.

subportion II-4 on a semi-preparative Phenomenex Luna PFP column (5 μm, 10 × 250 mm, Torrance, CA, USA) eluted by 50% MeCN, 2 mL/min, to afford **1** (185.7 mg, t_R = 9.36 min), **2** (237.6 mg, t_R = 17.99 min), and **3** (12.6 mg, t_R = 10.25 min). The same subportion was chromatographed by HPLC on the same column with 65% MeCN to give **5** (4.3 mg, t_R = 11.74 min). The subportion II-3 was purified by HPLC on a semi-preparative Thermo Hypersil HS C18 column (5 μm, 10 × 250 mm, Belle-fonte, PA, USA) eluted by 40% MeOH, 2 mL/min, to obtain **6** (7.7 mg, t_R = 25.59 min) and **7** (14.5 mg, t_R = 27.53 min). The same subportion was chromatographed on the same HPLC column eluted with 50% MeOH to give **4** (35.0 mg, t_R = 19.99 min).

2.3.1. Fimbriether A (1)

Amorphous white powder; $[\alpha]^{24}_D$ −6.5 (c 0.8, MeOH); IR (ZnSe) ν_{max} 3300−2600, 2927, 1687, 1604, 1510, 1426, 1249, 1168, 1102, 1020 cm^{-1}; UV λ_{max} (log ε, MeOH) 253 (4.2); ^{13}C and ^{1}H NMR data, see Tables 1 and 2; ESIMS [M − H]$^-$ m/z 221; HRESIMS [M − H]$^-$ m/z 221.0812 (calcd. for $C_{12}H_{13}O_4$, 221.0814).

2.3.2. Fimbriether B (2)

Amorphous white powder; $[\alpha]^{24}_D$ −10.9 (c 0.9, MeOH); IR (ZnSe) ν_{max} 3454, 2947, 1709, 1604, 1510, 1440, 1253, 1171, 1108, 1021 cm^{-1}; UV λ_{max} (logε, MeOH) 256 (4.2); ^{13}C and ^{1}H NMR data, see Tables 1 and 2; ESIMS [M + H]$^+$ m/z 237; HRESIMS [M + H]$^+$ m/z 237.1125 (calcd. for $C_{13}H_{17}O_4$, 237.1127).

2.3.3. Fimbriether C (3)

Amorphous white powder; $[\alpha]^{24}_D$ −14.4 (c 0.6, MeOH); IR (KBr) ν_{max} 3364, 2931, 2869, 1685, 1602, 1510, 1431, 1311, 1249, 1171, 1053, 1023 cm^{-1}; UV λ_{max} (logε, MeOH) 223 (4.1), 301 (4.3); ^{13}C and ^{1}H NMR data, see Tables 1 and 2; ESIMS [M − H]$^-$ m/z 247; HRESIMS [M − H]$^-$ m/z 247.0971 (calcd. for $C_{14}H_{15}O_4$, 247.0970).

2.3.4. Fimbriether D (4)

Amorphous white powder; $[\alpha]^{24}_D$ −16.6 (c 0.5, MeOH); IR (KBr) ν_{max} 3357, 2930, 2873, 1608, 1511, 1448, 1240, 1173, 1102, 1011 cm^{-1}; ^{13}C and ^{1}H NMR data, see Tables 1 and 2; ESIMS [M + H]$^+$ m/z 209; HRESIMS [M + H]$^+$ m/z 209.1174 (calcd. for $C_{12}H_{17}O_3$, 209.1178).

Table 1 − ^{13}C NMR spectroscopic data for compounds 1−7 (δ in ppm, mult.).

No.	1[a,b]	2[a,b]	3[a,b]	4[a,b]	5[a,b]	6[a,b]	7[a,b]
1	124.5 s	123.7 s	128.8 s	135.1 s	123.6 s	123.5 s	123.6 s
2	132.8 d	132.5 d	130.8 d	129.6 d	132.6 d	132.6 d	132.6 d
3	115.3 d	115.4 d	116.1 d	115.6 d	115.4 d	115.5 d	115.4 d
4	164.2 s	164.3 s	162.2 s	159.7 s	164.6 s	164.7 s	164.6 s
5	115.3 d	115.4 d	116.1 d	115.6 d	115.4 d	115.5 d	115.4 d
6	132.8 d	132.5 d	130.8 d	129.6 d	132.6 d	132.6 d	132.6 d
7	170.0 s	168.4 s	145.6 d	64.9 t	168.5 s	168.5 s	168.5 s
8			117.4 d				
9			171.3 s				
-OMe		52.3 q			52.3 q	52.3 q	52.3 q
1′	72.2 t	72.2 t	72.2 t	72.2 t	75.6 t	70.9 t	70.7 t
2′	74.5 d	74.5 d	74.6 d	74.7 d	72.0 d	73.9 d	75.1 d
3′	145.8 s	145.8 s	145.9 s	146.1 s	32.1 d	74.6 s	74.7 s
4′	113.0 t	113.0 t	112.9 t	112.8 t	18.1 q	19.4 q	21.6 q
5′	18.8 q	18.8 q	18.8 q	18.8 q	19.4 q	68.5 t	67.9 t

[a] Measured in methanol-d_4 (125 MHz).
[b] Multiplicities were obtained from phase-sensitive HSQC experiments.

Table 2 − ^{1}H NMR spectroscopic data for compounds 1−7 [δ in ppm, mult. (J in Hz)].

No.	1[a]	2[a]	3[a]	4[a]	5[a]	6[a]	7[a]
2	7.96 d (8.7)	7.94 d (8.9)	7.53 d (8.7)	7.26 d (8.7)	7.96 d (8.7)	7.96 d (8.8)	7.96 d (8.8)
3	6.99 d (8.7)	7.00 d (8.9)	6.98 d (8.7)	6.92 d (8.7)	7.02 d (8.7)	7.03 d (8.8)	7.03 d (8.8)
5	6.99 d (8.7)	7.00 d (8.9)	6.98 d (8.7)	6.92 d (8.7)	7.02 d (8.7)	7.03 d (8.8)	7.03 d (8.8)
6	7.96 d (8.7)	7.94 d (8.9)	7.53 d (8.7)	7.26 d (8.7)	7.96 d (8.7)	7.96 d (8.8)	7.96 d (8.8)
7			7.60 d (15.9)	4.52 s			
8			6.34 d (15.9)				
-OMe		3.85 s			3.86 s	3.87 s	3.87 s
1′	4.01 dd (9.9, 7.2)	4.01 dd (9.9, 7.2)	3.99 dd (9.9, 7.2)	3.94 dd (9.9, 7.1)	4.00 dd (9.9, 6.6)	4.07 dd (10.0, 8.3)	4.07 dd (10.1, 8.0)
	4.09 dd (9.9, 4.0)	4.09 dd (9.9, 3.9)	4.07 dd (9.9, 4.0)	4.02 dd (9.9, 4.1)	4.09 dd (9.9, 3.6)	4.38 dd (10.0, 2.2)	4.35 dd (10.1, 2.8)
2′	4.41 dd (7.2, 4.0)	4.41 dd (7.2, 3.9)	4.39 dd (7.2, 4.0)	4.38 dd (7.1, 4.1)	3.68 dd (6.6, 3.6)	3.98 dd (8.3, 2.2)	3.94 dd (8.0, 2.8)
3′					1.90 m		
4′	4.96 s	4.97 s	4.97 s	4.95 br s	1.01 d (6.9)	1.19 s	1.23 s
	5.10 s	5.11 s	5.10 s	5.09 br s			
5′	1.81 s	1.81 s	1.82 s	1.81 s	1.00 d (6.9)	3.48 d (11.1)	3.54 d (11.1)
						3.61 d (11.1)	3.60 d (11.1)

[a] Measured in methanol-d_4 (500 MHz).

2.3.5. Fimbriether E (5)

Amorphous white powder; $[\alpha]^{24}_D$ −16.2 (c 0.6, MeOH); IR (KBr) ν_{max} 3492, 2959, 1712, 1605, 1510, 1442, 1257, 1172, 1110, 1056 cm^{-1}; UV λ_{max} (log ε, MeOH) 257 (4.3); ^{13}C and ^{1}H NMR data, see Tables 1 and 2; ESIMS [M + H]$^+$ m/z 239; HRESIMS [M + H]$^+$ m/z 239.1280 (calcd. for C$_{13}$H$_{19}$O$_4$, 239.1283).

2.3.6. Fimbriether F (6)

Amorphous white powder; $[\alpha]^{24}_D$ +35.8 (c 0.5, MeOH); IR (KBr) ν_{max} 3435, 2933, 2860, 1694, 1674, 1621, 1442,1373, 1318, 1238, 1197 cm^{-1}; UV λ_{max} (log ε, MeOH) 210 (4.1), 256 (4.3); ^{13}C and ^{1}H NMR data, see Tables 1 and 2; ESIMS [M + Na]$^+$ m/z 293; HRESIMS [M + Na]$^+$ m/z 293.1003 (calcd. for C$_{13}$H$_{18}$O$_6$Na, 293.1001).

2.3.7. Fimbriether G (7)

Amorphous white powder; $[\alpha]^{24}_D$ +30.6 (c 0.4, MeOH); IR (KBr) ν_{max} 3404, 2948, 1705, 1604, 1510, 1440, 1254, 1172, 1110, 1023 cm^{-1}; UV λ_{max} (log ε, MeOH) 210 (4.1), 257 (4.2); ^{13}C and ^{1}H NMR data, see Tables 1 and 2; ESIMS [M + Na]$^+$ m/z 293; HRESIMS [M + Na]$^+$ m/z 293.1004 (calcd. for C$_{13}$H$_{18}$O$_6$Na, 293.1001).

2.4. Nitrite measurement and cell viability assay

The methods were essentially the same as reported previously [17]. Briefly, RAW 264.7 cell line was obtained from the Bioresource Collection and Research Center (Hsinchu, Taiwan) were maintained in Dulbecco's modified Eagle medium supplemented with 10% fetal calf serum and penicillin-streptomycin. Cell aliquots were seeded in 24-well plate for 24 h and then changed to serum-free media for 4 h to render the attached cells quiescence. To assess the effects on LPS-induced NO production, compounds 1−7 and two positive control aminoguanidine (a specific inhibitor of iNOS), N^{ω}-nitro-L-arginine (L-NNA, a non-selective NOS inhibitor) or vehicle (0.1%, DMSO) were added in the presence of LPS (200 ng/mL) to the cells for further 24 h. The nitrite concentration in the culture medium was determined spectrophotometrically as an index of NO production by Griess reaction [18]. The adhered cells were added with 10% alamarBlue in medium for another 3 h in the humidified 5% CO$_2$ incubator. The absorbance of the supernatants was read at 575 and 595 nm on a microplate reader (BioTek, Winooski, VT, USA). Both positive controls were purchased from Sigma−Aldrich Chemical Co., and the purity of each compound was more than 98%.

2.5. Aortic ring preparations and relaxation on phenylephrine-induced contraction

The method was essentially the same as published previously by our laboratory [19]. All procedures were approved by the Laboratory Animal Service Center, China Medical University (Taichung, Taiwan), and animal care was conducted in accordance with the center's Institutional Animal Ethical Guidelines. The thoracic aorta was excised from C57BL/6J mouse and fixed isometrically in organ chambers containing oxygenated Krebs' solution. After equilibration, a relaxation (more than 70%) induced by acetylcholine (1 μM) in aortic rings precontracted with phenylephrine (1 μM) indicated the intact endothelium. For the evaluation of relaxation, test compound was added individually during the tonic phase of contraction (considered as 100%) induced by phenylephrine (1 μM).

2.6. Statistical analysis

Data are given as mean ± S.E. and n represents the number of independently performed experiments. Comparisons of the treatment effects were made using ANOVA, followed by post hoc comparisons using Newman−Keuls test as appropriate. P value less than 0.05 was considered to indicate a statistically significant difference.

3. Results and discussion

From the ethyl acetate extracts of the fermented broths of X. fimbriata YMJ491, seven previously unreported compounds 1−7 were isolated and purified by successive Sephadex LH-20 open column and semi-preparative reversed phase HPLC, and their structures were further elucidated by spectroscopic data and compared with the literature.

Compound 1 was afforded as an amorphous white powder with a molecular formula of C$_{12}$H$_{14}$O$_4$, which was determined by negative mode HRESIMS and supported by ^{13}C NMR assignments (Table 1). The IR spectrum exhibited the absorption bands at 3300−2600 coupled with 1687 and 1604 and 1510 cm^{-1}, indicating the presence of a conjugated carboxylic acid and a benzene ring, respectively. The ^{1}H NMR spectrum shows typical resonances for a 1,4-disubstituted phenyl AA'XX'-type mutually coupled signals at δ_H 6.99 (2H, d, J = 8.7 Hz, H-3, -5) and 7.96 (2H, d, J = 8.7 Hz, H-2, -6), an exomethylene signals at δ_H 4.96 and 5.10 (each 1H, s, H$_2$-4′), three carbinoyl proton signals at δ_H 4.01 (1H, dd, J = 9.9, 7.2 Hz, H$_a$-1′), 4.09 (1H, dd, J = 9.9, 4.0 Hz, H$_b$-1′), and 4.41 (1H, dd, J = 7.2, 4.0 Hz, H-2′), and a methyl signals at δ_H 1.81 (3H, s, H$_3$-5′) attached to an olefinic functionality (Table 2). The ^{13}C NMR spectrum coupled with phase-sensitive HSQC spectrum of 1 showed 12 carbon signals for one methyl at δ_C 18.8 (C-5′), two methylenes at δ_C 72.2 (C-1′) and 113.0 (C-4′), five methines at δ_C 74.5 (C-2′), 115.3 (C-3 and -5), and 132.8 (C-2 and -6), and four non-protonated carbons at δ_C 124.5 (C-1), 145.8 (C-3′), 164.2 (C-4), and 170.0 (C-7) (Table 1). Above NMR data suggested 1 had a structural feature almost compatible with that of stachyline B, a putative tyrosine-derived and O-prenylated chemical entity, isolated from the sponge-derived fungus Stachylidium sp. [20], except that the lack of a methylene functionality attached to the phenyl moiety. The gross structure of 1 was further confirmed by key cross-peaks of δ_H 6.99 (H-3, -5)/δ_H 7.96 (H-2, -6) and δ_H 4.01, 4.09 (H$_2$-1′)/δ_H 4.41 (H-2′) in the COSY spectrum accompanied by key long−range correlations of δ_H 1.81 (H$_3$-5′)/δ_C 74.5 (C-2′) and 113.0 (C-4′), δ_H 4.01, 4.09 (H$_2$-1′)/δ_C 164.2 (C-4), and δ_H 7.96 (H-2, -6)/δ_C 170.0 (C-7) in the HMBC spectrum (Fig. 2). The absolute configurations of the only chiral center C-2′ in 1 was deduced to be S form on the basis of the same sign of the specific optical rotation value ($[\alpha]^{24}_D$ −6.5) in comparison with that of its analogue stachyline B ($[\alpha]^{23}_D$ −12.0) [20]. Thus, the structure of 1 was established as shown in Fig. 1, and was named fimbriether A.
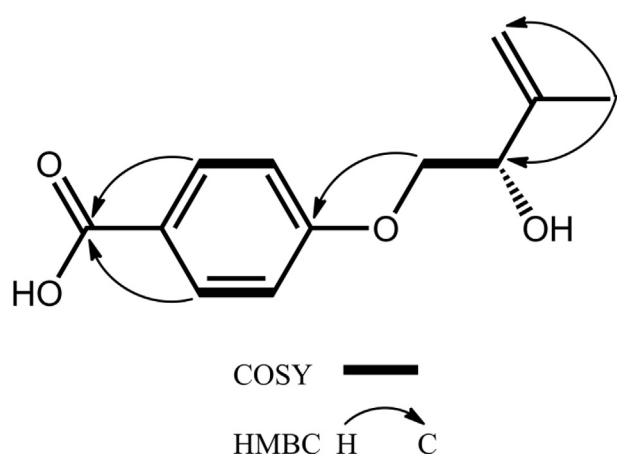
Fig. 2 – Key COSY and HMBC correlations of **1**.

The molecular formula of **2** was determined to be $C_{13}H_{16}O_4$, 14 Da more than that of **1**, by HRESIMS and ^{13}C NMR (Table 1). The ^{13}C and ^{1}H NMR spectra of **2** were consistent with those of **1** except that an additional methyl signal at δ_C 52.3 and δ_H 3.85, was observed, and δ_C170 (C-7) in **1** upfield shifted to δ_C 168.4 (C-7) in **2**. In the HMBC spectrum of **2**, a conspicuous cross-peak of δ_H 3.85/δ_C 168.4 (C-7) corroborated the location of the methoxyl group at C-7. The absolute configuration of C-2′ in **2** was confirmed to be the same with that of compound **1** due to the same sign of the specific optical rotation values. Accordingly, compound **2** was assigned to be a methyl ester of **1**.

The molecular formula of **3** was deduced by HRESIMS and ^{13}C NMR to be $C_{14}H_{16}O_4$, requiring double bond equivalents of seven, which indicated one more double bond than that of **1**. The ^{13}C and ^{1}H NMR data of **3** coincided well with those of **1** except that two additional *trans*-coupled double bond signals at δ_C 117.4, 145.6 and δ_H 6.34 (1H, d, J = 15.9 Hz), 7.60 (1H, d, J = 15.9 Hz), respectively, appeared in **3**, and δ_C170 (C-7) in **1** downfield shifted to δ_C 171.3 (C-9) in **3**. Its UV absorption maxima at 223 and 301 nm also indicated a *trans*-phenyl-propenoic acid skeleton [21], which was further supported by key cross-peaks of H-7/C-2, -6, and -9 and H-8/C-1 and -9 in the HMBC spectrum of **3**. The absolute configuration of the asymmetric C-2′ in **3** was determined to be S form by the negative specific optical rotation value ($[\alpha]^{24}_D$ −14.4) when compared to that of compound **1**. Therefore, compound **3** was identified to be (S,E)-3-(4-((2-hydroxy-3-methylbut-3-en-1-yl)oxy)phenyl)acrylic acid, and was named fimbriether C.

The IR spectrum of **4** indicated the presence of a hydroxy (3357 cm^{-1}) and a benzene ring (1608 and 1511 cm^{-1}). Its ^{13}C and ^{1}H NMR data were in accordance with those of **1** except that a carboxylic acid group at δ_C 170.0 in **1** was substituted by −CH$_2$-OH at δ_C 64.9 and δ_H 4.52, respectively, in **4** as evidenced from the molecular formula of $C_{12}H_{16}O_3$, 14 Da less than that of **1**, as deduced from HRESIMS and ^{13}C NMR (Table 1). Compound **4** had the S-absolute configuration at C-2′ since it showed the same sign of $[\alpha]^{24}_D$ −16.6 with that of compound **1**. Thus, compound **4** was determined to be an O-prenylated p-phenylmethyl alcohol as shown in Fig. 1.

The ^{13}C and ^{1}H NMR spectra of **5** were in agreement with those of **2** except that the exomethylene signals at δ_C 113.0 (C-4′), 145.8 (C-3′) and δ_H 4.97, 5.11 (each1H, s, H$_2$-4′), respectively,

in **2** were reduced to be a methyl [δ_C 18.1 (C-4′); δ_H 1.01 (3H, d, J = 6.9 Hz, H$_3$-4′)] coupled with a methine group [δ_C 32.1 (C-3′); δ_H 1.90 (1H, m, H-3′)] in **5**. The difference was also reflected in their MS data that **5** adopting a molecular formula of $C_{13}H_{18}O_4$ was 2 Da more than that of **2**. The chirality of C-2′ in **5** was assigned to be S-form based on the same negative specific optical rotation ($[\alpha]^{24}_D$ −16.2) with that of compound **2**. Hence, the structure of **5** was established to be (S)-methyl 4-(2-hydroxy-3-methylbutoxy)benzoate, and was named as fimbriether E.

Both compounds **6** and **7** adopted the same molecular formula of $C_{13}H_{18}O_6$, 32 Da more than that of **5**, as determined by HRESIMS and ^{13}C NMR (Table 1). Their UV absorption maxima at around 257 nm, the same with those of **2** and **5**, and similar aromatic resonances in the ^{13}C and ^{1}H NMR spectra (Tables 1 and 2) indicated **6** and **7** shared the same benzoyl chromophore with that of **2** and **5**. From comparison of ^{13}C NMR data of **5–7**, the chemical shifts of the C-3′ and C-5′ downfield shifted dramatically from δ_C 32.1 and 19.4, respectively, in **5** to δ_C 65.0–75.0 attributable to oxygenated C-3′ and C-5′ in both **6** and **7**. Key cross-peaks of H$_2$-5′/C-2′ and -4′ and H$_3$-4′/C-2′ and C-5′ in the HMBC spectrum together with key cross-peaks of H$_2$-1′/H-2′ in the COSY spectrum (Fig. 3) also supported that **6** and **7** were 3′,5′-dihydroxy analogues of **5**. The chemical shifts of the C-3′–C-5′ moiety of **6** at δ_C 74.6, 19.4, and 68.5, respectively, were compatible with those of 2-C-methyl-D-erythritol (Fig. 4) [22]. Thus, the relative configurations of C-2′ and C-3′ in **6** was verified to be R* and S* forms, respectively. The chemical shifts of the C-3′–C-5′ moiety of **7** at δ_C 74.7, 21.6, and 67.9, respectively, were coincided well with those of 2-C-methyl-D-threitol (Fig. 4) [22]. Therefore, the relative configurations of C-2′ and C-3′ in **7** was determined to be both R* forms. Unambiguously, the structures of **6** and **7** were characterized as shown in Fig. 1, and were named as fimbriethers F and G, respectively.

Several lines of evidence indicate that NO has been involved in the pathogenesis of various chronic inflammatory diseases, such as rheumatoid arthritis [23], inflammatory bowel disease [24], diabetic retinopathy [25], cancer metastasis [26], and lung fibrosis [27]. In the present study, we set out to elucidate the anti-inflammatory activity of compounds **1–7** by assessment of their inhibition on NO production in LPS-activated murine macrophage RAW264.7 cells. Of the compounds estimated, **7** exhibited the strongest NO inhibition with the average maximum inhibition (Emax) at 100 μM of
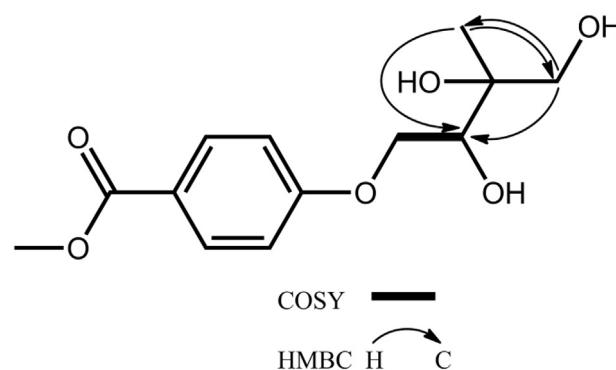

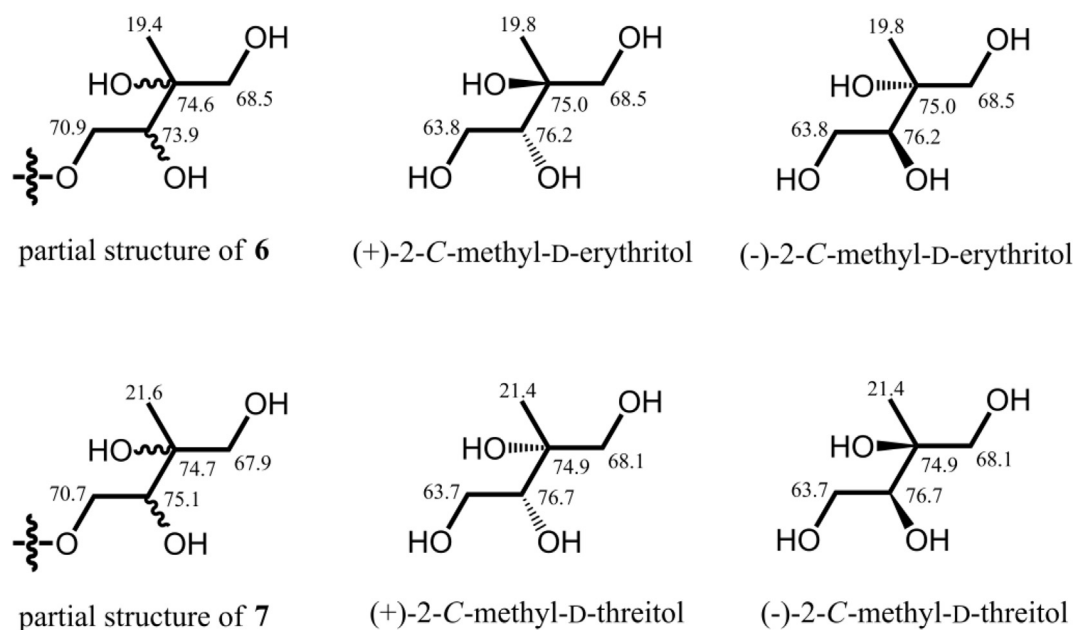**Fig. 3** – Key COSY and HMBC correlations of **6** and **7**.

Fig. 4 — ^{13}C NMR data of the C-1′–C-5′ moiety of 6, 7, and literature data.

49.7 ± 0.5%. The results are comparable with the positive control N^{ω}-nitro-L-arginine (Table 3). Compounds **2** and **5** showed moderate iNOS inhibitory activity, with E_{max} values of 31.3 ± 1.3% and 38.9 ± 0.1%, respectively. In contrast, the other 4 isolates seem not to be linked to NO production at the test concentration. In addition, none of the compounds (up to 100 μM) was found to significantly affect the cell viability of RAW264.7 cells. In another series of experiments, all test compounds did not alter phenylephrine-induced vaso-contraction in isolated thoracic aortic rings of the C57BL/6J mouse, indicating **1–7** is not involved in the regulation of endothelial NOS-mediated NO production (data not shown). These results suggested that the **2**, **5**, and **7** play a specific role

in the anti-inflammatory activity of the termite nest-derived medicinal fungus *X. fimbriata* YMJ491. It seemed that compounds **2**, **5**, and **7** share the same structural feature of methyl benzoate moiety indicating a possible active site. Compound **6** with the same functionality exhibiting a sharp decrease of NO production inhibitory activity demonstrated the stereochemistry of C-3′ is as important as methyl benzoate moiety.

4. Conclusion

In this report, we have identified seven new isoprenyl phenolic ethers from *Xylaria fimbriata* YMJ491. To date, fungal natural products with such skeletal type are rare. Of the compounds identified, **2**, **5**, and **7** can inhibit NO production of RAW264.7 cells to a certain extent without significant cyto-toxicity, and may provide a rationale for the potential medicinal uses of *Xylaria fimbriata* YMJ491 as anti-inflammatory agents.

Conflicts of interest

The authors declare that there are no potential conflicts of interest.

Acknowledgments

Table 3 — The effects of compounds 1–7 isolated from *Xylaria fimbriata* on nitrite production and cell viability in LPS-activated RAW264.7 cells.

Compounds	E_{max} (%)[a]	Cell viability (%)
Fimbriether A (**1**)	4.6 ± 2.0	94.3 ± 0.5
Fimbriether B (**2**)	31.3 ± 1.3*	94.1 ± 1.4
Fimbriether C (**3**)	7.7 ± 5.9	91.2 ± 2.2
Fimbriether D (**4**)	7.3 ± 2.8	95.3 ± 2.5
Fimbriether E (**5**)	38.9 ± 0.1*	92.8 ± 2.0
Fimbriether F (**6**)	6.0 ± 3.9	92.1 ± 1.7
Fimbriether G (**7**)	49.7 ± 0.5*	91.2 ± 2.2
Aminoguanidine[b]	83.7 ± 0.3*	99.2 ± 1.6
N^{ω}-nitro-L-arginine[c]	42.1 ± 0.4*	101.7 ± 2.2

*$P < 0.05$ when compared with vehicle-treated group.
[a] E_{max} indicates the mean maximum inhibitory effect at a concentration of 100 μM, expressed as the percentage inhibition of nitrite production induced by LPS (200 ng/mL) in the presence of vehicle.
[b] Positive control: a selective iNOS inhibitor.
[c] Positive control: a non-selective iNOS inhibitor. $n = 3–4$ in each group.

Appendix A. Supplementary data

Supplementary data related to this article can be found at https://doi.org/10.1016/j.jfda.2018.05.007.

REFERENCES

[1] Aanen DK, Eggleton P, Rouland-Lefèvre C, Guldberg-Frøslev T, Rosendahl S, Boomsma JJ. The evolution of fungus-growing termites and their mutualistic fungal symbionts. Proc Natl Acad Sci Unit States Am 2002;99:14887–92.

[2] Rogers JD, Ju YM, Lehmann J. Some *Xylaria* species on termite nests. Mycologia 2005;97:914–23.

[3] Chang JC, Hsiao G, Lin RK, Kuo YH, JuYM Lee TH. Bioactive constituents from the termite nest-derived medicinal fungus *Xylaria nigripes*. J Nat Prod 2017;80:38–44.

[4] Ju YM, Hsieh HM. *Xylaria* species associated with nests of *Odontotermes formosanus* in Taiwan. Mycologia 2007;99:936–57.

[5] Liang WL, Hsiao CJ, Ju YM, Lee LH, Lee TH. Chemical constituents of the fermented broth of the ascomycete *Theissenia cinerea* 89091602. Chem Biodivers 2011;8:2285–90.

[6] Somboon P, Poonsawad A, Wattanachaisaereekul S, Jensen LT, Niimi M, Cheevadhanarak S, et al. Fungicide *Xylaria* sp. BCC 1067 extract induces reactive oxygen species and activates multidrug resistance system in *Saccharomyces cerevisiae*. Future Microbiol 2017;12:417–40.

[7] Xu WF, Hou XM, Yao FH, Zheng N, Li J, Wang CY, et al. Xylapeptide A, an antibacterial cyclopentapeptide with an uncommon L-pipecolinic acid moiety from the associated fungus Xylaria sp. (GDG-102). Sci Rep 2017;7:6937–44.

[8] Macías-Rubalcava ML, Sánchez-Fernández RE. Secondary metabolites of endophytic *Xylaria* species with potential applications in medicine and agriculture. World J Microbiol Biotechnol 2017;33:15–36.

[9] Kim TY, Jang JY, Yu NH, Chi WJ, Bae CH, Yeo JH, et al. Nematicidal activity of grammicin produced by *Xylaria grammica* KCTC 13121BP against *Meloidogyne incognita*. Pest Manag Sci 2018;74:384–91.

[10] Pan N, Lu LY, Wang GH, Sun FY, Sun HS, Wen XJ, et al. Xyloketal B alleviates cerebral infarction and neurologic deficits in a mouse stroke model by suppressing the ROS/TLR4/NF-κB inflammatory signaling pathway. Acta Pharmacol Sin 2017;38:1236–47.

[11] Guo C, Wu P, Xue J, Li H, Wei X. Xylaropyrones B and C, new γ-pyrones from the endophytic fungus *Xylaria* sp. SC1440. Nat Prod Res 2017. https://doi.org/10.1080/14786419.2017.1385013.

[12] Lei CW, Yang ZQ, Zeng YP, Zhou Y, Huang Y, He XS, et al. A new cytochalasan from the fungus *Xylaria striata*. Nat Prod Res 2018;32:7–13.

[13] McCloskey S, Noppawan S, Mongkolthanaruk W, Suwannasai N, Senawong T, Prawat U. A new cerebroside and the cytotoxic constituents isolated from *Xylaria allantoidea* SWUF76. Nat Prod Res 2017;31:1422–30.

[14] Tchoukoua A, Ota T, Akanuma R, Ju YM, Supratman U, Murayama T, et al. A phytotoxic bicyclic lactone and other compounds from endophyte *Xylaria curta*. Nat Prod Res 2017;31:2113–8.

[15] Zheng N, Yao F, Liang X, Liu Q, Xu W, Liang Y, et al. A new phthalide from the endophytic fungus *Xylaria* sp. GDG-102. Nat Prod Res 2018;32:755–60.

[16] Hsieh HM, Lin CR, Fang MJ, Rogers JD, Fournier J, Lechat C, et al. Phylogenetic status of *Xylaria* subgenus *Pseudoxylaria* among taxa of the subfamily Xylarioideae (Xylariaceae) and phylogeny of the taxa involved in the subfamily. Mol Phylogenet Evol 2010;54:957–69.

[17] Chang YC, Lu CK, Chiang YR, Wang GJ, Ju YM, Kuo YH, et al. Diterpene glycosides and polyketides from *Xylotumulus gibbisporus*. J Nat Prod 2014;77:751–7.

[18] Green LC, Wagner DA, Glogowski J, Wishnik IS, Tannenbaum SR. Analysis of nitrate, nitrite, and [^{15}N]nitrate in biological fluids. Anal Biochem 1982;126:131–8.

[19] Lin YL, Yet SF, Hsu YT, Wang GJ, Hung SC. Mesenchymal stem cells ameliorate atherosclerotic lesions via restoring endothelial function. Stem Cells Transl Med 2015;4:44–55.

[20] Almeida C, Part N, Bouhired S, Kehraus S, König GM. Stachylines A–D from the sponge-derived fungus *Stachylidium* sp. J Nat Prod 2011;74:21–5.

[21] Lee TH, Huang NK, Lai TC, Yang ATY, Wang GJ. Anemonin, from *Clematis crassifolia*, potent and selective inducible nitric oxide synthase inhibitor. J Ethnopharmacol 2008;116:518–27.

[22] Ghosh SK, Butler MS, Lear MJ. Synthesis of 2-C-methylerythritols and 2-C-methylthreitols via enantiodivergent sharpless dihydroxylation of trisubstituted olefins. Tetrahedron Lett 2012;53:2706–8.

[23] Negi VS, Mariaselvam CM, Misra DP, Muralidharan N, Fortier C, Charron D, et al. Polymorphisms in the promoter region of iNOS predispose to rheumatoid arthritis in south Indian Tamils. Int J Immunogenet 2017;44:114–21.

[24] Qidwai T, Jamal F. Inducible nitric oxide synthase (iNOS) gene polymorphism and disease prevalence. Scand J Immunol 2010;72:375–87.

[25] Warpeha KM, Xu W, Liu L, Charles IG, Patterson CC, Ah-Fat F, et al. Genotyping and functional analysis of a polymorphic (CCTTT)(n) repeat of NOS2A in diabetic retinopathy. FASEB J 1999;13:1825–32.

[26] Lee SH, Jaganath IB, Atiya N, Manikam R, Sekaran SD. Suppression of ERK1/2 and hypoxia pathways by four *Phyllanthus* species inhibits metastasis of human breast cancer cells. J Food Drug Anal 2016;24:855–65.

[27] Chang CW, Lin CC, Lien HY, Lin YC, Chen YH, Chang FR, et al. Effects of Ma-Xing-Shi-Gan-Tang on bleomycin-induced lung fibrosis in rats. J Food Drug Anal 2011;19:139–45.